JOURNAL OF MATERIALS SCIENCE 22 (1987) 4465–4469

Yttria migration in Y–TZP during high-temperature annealing

P. J. WHALEN, F. REIDINGER, S. T. CORREALE, J. MARTI
Allied Signal Inc., Corporate Research, Morristown, New Jersey, USA

The microstructural and phase changes occurring during the high temperature (1300 to 1550° C) annealing of Y–TZP were studied using X-ray fluorescence, X-ray diffraction, and TEM. Two processes occurred simultaneously involving the diffusion of yttrium. The Y–TZP partitioned into yttria-rich and yttria-poor phases throughout the material, because the material lies in a two-phase field of the yttria-zirconia phase diagram. The other process involved the segregation of yttrium to the surface, the extent of which was shown to vary with the state of the surface (ground or polished), annealing temperature, and silica content. Migration of yttrium to the surface caused a significant surface composition change (i.e. from 4.7 wt% Y_2O_3 at room temperature to 8.9 wt% Y_2O_3 at 1550° C for 3 h), resulting in a microstructure and phase composition different from the bulk.

1. Introduction

Zirconia ceramics are being considered for a wide range of both high- ($\leqslant 1000°$ C) and room-temperature applications as structural components, because of their outstanding strength and toughness. In the special case of 100% tetragonal yttria–zirconia (Y–TZP), small changes in chemical composition (yttria content) and grain size can have a deleterious effect on the mechanical properties of the material [1]. It is essential that these changes do not occur in the temperature range where the material is destined for use.

The need for a detailed X-ray fluorescence and diffraction study became apparent when we observed unexpected variations in the elemental and phase compositions, i.e. Y/Zr and cubic/tetragonal ratios, in nominally 4.5 wt% Y_2O_3–ZrO_2 "single"-phase tetragonal ceramics. These observations could not be explained by equilibrium phase diagrams of this system, so chemical changes or non-equilibrium effects were suspected. The changes were dominant on the surface during higher temperature ($> 1300°$ C) anneals. The XRF technique exploits the different penetration depths of the *L* and *K* radiation of yttrium to probe the near surface region ($< 1\,\mu m$) and deep surface region ($\sim 40\,\mu m$) for yttrium content. In addition, a careful analysis of relevant XRD patterns shows interesting phase compositions resulting from these chemical changes.

The analyses were performed on sintered tetragonal zirconia (~ 2.4 mol% Y_2O_3) fabricated from two different commercial powders. The effect of surface grinding and annealing temperature on yttria concentration was studied.

2. Experimental technique

The powders used in this study were obtained from two large zirconia suppliers. The first material (Toyo Soda, TZ-2.5, Atlanta, Georgia), designated Lo-Sil in this study, contained 4.45 wt% Y_2O_3, 0.068 wt% Al_2O_3, 0.008 wt% SiO_2, 0.002 wt% Fe_2O_3 and 0.001 wt% Na_2O_3. This powder was received in the form of 30 to 70 μm spray-dried spheres. Another commercial powder (Zircar, ZYP-4.5, Florida, New York), labelled Hi-Sil, was analysed by XRF and wet chemistry and shown to contain between 4.7 and 4.8 wt% Y_2O_3, and a significantly higher silica content (approximately four times that of the Lo-Sil). The powders were used as-received; there was no milling before processing. Both powders were cold isostatically pressed into 2.0 cm diameter cylinders at 275 MPa. The cylinders were fired to > 98% theoretical density (5.99 g cm^{-3}) at 1375° C for 3 h. After sintering, the cylinders were sliced into discs approximately 2.0 mm thick. The discs were then surface ground using a 220 M diamond wheel on one side and polished down to a 1 μm diamond paste (3×10^{-3} in. finish) on the other.

Discs from each powder were then heat treated for 3 h at temperatures ranging from 1300 to 1550° C in air, and cooled at 300° C h^{-1} to room temperature. A Philips diffractometer (APD 3600) with a graphite exit beam monochromator and Cu$K\alpha$ radiation at 45 kV and 40 mA was used to analyse the various phase

TABLE I X-ray fluorescence experimental conditions

	Emission line			
	Zr$K\alpha$	Y$K\alpha$	Zr$L\alpha$	Y$L\alpha$
Peak 2θ (deg)	22.495	23.730	87.835	94.945
Background 2θ	−0.8, +1.0	−0.6, +0.8	−2.	−2.
Crystal	LIF (200)	LIF (200)	PET	PET
Collimator	Fine	Fine	Fine	Fine
Detector	S*	S	F†	F
Counts peak	500 000	500 000	50 000	50 000
Counts bkgnd.	10 000	10 000	10 000	10 000
kV, mA	50, 40	50, 40	60, 50	60, 50

*S, NaI(Th) scintillation detector
†F, Flow proportional counter using P10 gas.

0022–2461/87 $03.00 + .12

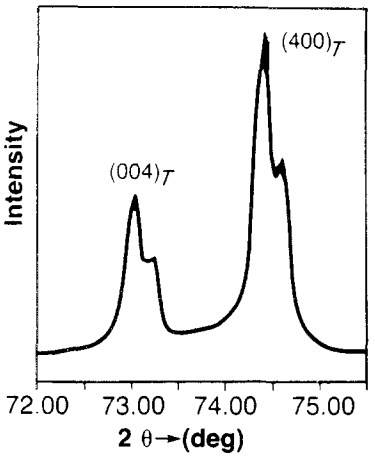

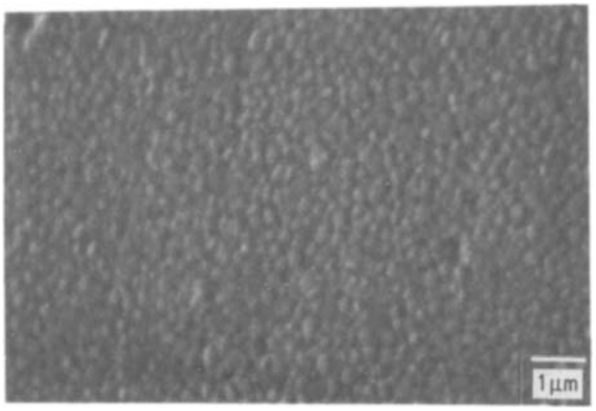

Figure 1 XRD pattern and thermally etched surface of Hi-Sil Y–TZP fired at 1375° C for 3 h.

compositions. Transmission electron microscopy and elemental analysis were performed with a Hitachi H800 TEM, fitted with a TN 5500 energy dispersive X-ray system.

The XRF analysis was performed using a Philips PW 1400 spectrometer with a rhodium X-ray tube operating at 60 kV and 50 mA for the $L\alpha$ measurements and at 50 kV and 40 mA for the $K\alpha$ measurements in a vacuum path. All experimental conditions are given in Table I. The Philips data collection software was used to run the analysis under the predescribed conditions and to print out the background corrected count rates which were used in the quantitative analysis. The measurements of the $K\alpha$ and $L\alpha$ lines were done by using fixed counts of 500 000 and 50 000, respectively, and 10 000 for the backgrounds in order to have statistical errors of less than 1%. As the total measurement time was several hours long, the standards were run several times through the course of the analysis to monitor any long-term fluctuations. The Criss Software (Criss Software, Inc., Largo, Maryland) XRF-11 fundamental parameters programs were used to do the quantitative analysis.

The comparison of the Y_2O_3 content between the bulk and the near surface region is possible due to the different effective penetration depths of the Y$K\alpha$ and Y$L\alpha$ emission signals. The effective mass absorption coefficient for the $K\alpha$ and $L\alpha$ emission lines were calculated considering the Rh$K\alpha$ line as the primary source of excitation for 4.5 wt % Y_2O_3/ZrO_2 according to the equation:

$$(\mu/\varrho) = (\mu/\varrho)\lambda_{\text{pri}} \csc\phi + (\mu/\varrho)_{\text{A}} \csc\chi$$

where $\csc\phi$ and $\csc\chi$ are the path lengths in the specimen, and $(\mu/\varrho)\lambda_{\text{pri}}$ and (μ/ϱ) are the mass absorption coefficients for the primary beam and the analyte line, respectively. The effective depths were calculated for two I/I_0 ratios using the equation:

$$x = \ln (I/I_0)/\mu$$

For $I/I_0 = 0.5$ the effective depths are 10 and $< 1\ \mu$m for the $K\alpha$ and $L\alpha$ lines, respectively, and approximately 70 and 5 μm when I/I_0 is 1/100. In either case, the depth being analysed is at least ten times greater for the $K\alpha$ lines than the $L\alpha$ lines; therefore the $L\alpha$ lines are more sensitive to the surface composition.

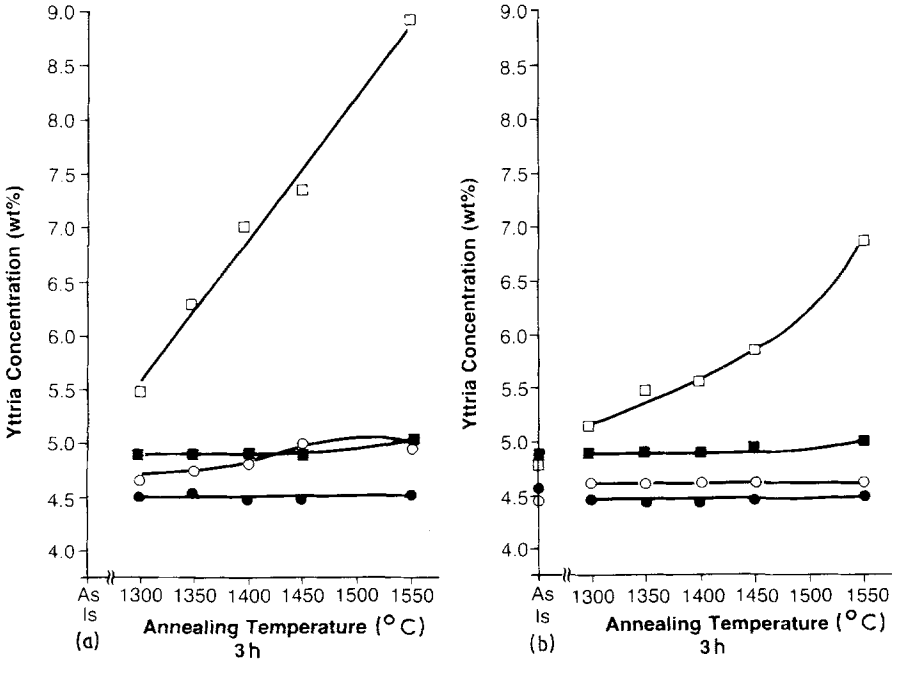

Figure 2 Yttria content in annealed Y–TZP ground surfaces; (a) machined, (b) polished. Lo-Sil: (○) L-radiation, (●) K-radiation. Hi-Sil: (□) L-radiation, (■) K-radiation.

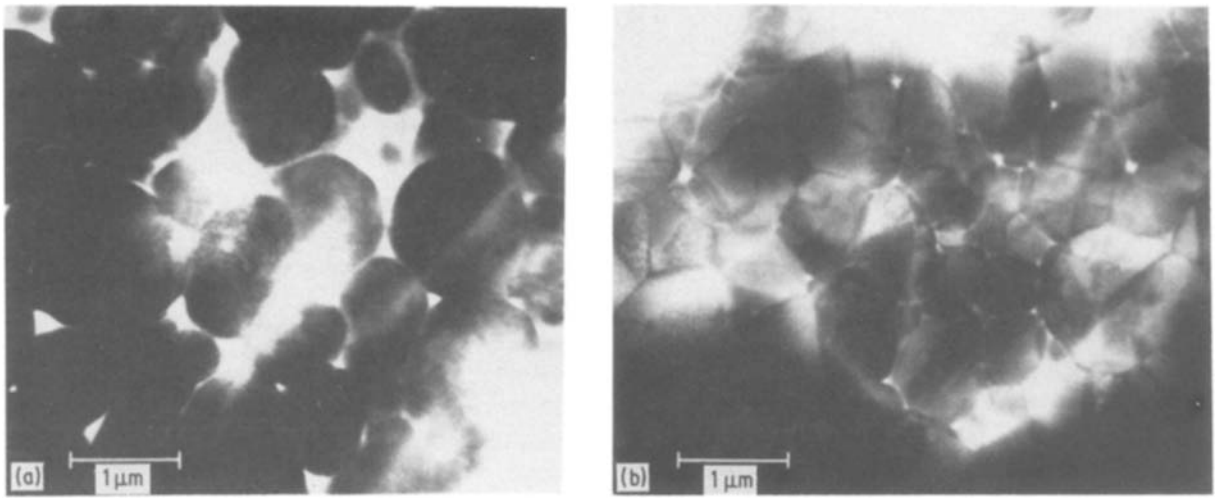

Figure 3 Microstructure of bulk (interior) region of samples annealed at 1550° C for 3 h: (a) Hi-Sil, (b) Lo-Sil.

3. Results and discussion

A polished and etched sample (1300° C/1 h) of the sintered Hi-Sil material is shown in Fig. 1. The XRD pattern shows only tetragonal phase in these uniform 0.5 μm grains. The as-fired Lo-Sil material had an identical microstructure and phase composition. The yttria content determined from the K and L lines of both materials was the same for the polished and ground sides of the as-fired samples. After annealing above 1300° C, the surface yttria content changed markedly in the Hi-Sil samples and only slightly in the Lo-Sil material, Fig. 2. The degree of yttria enrichment was significantly higher on the ground surfaces compared to the polished surfaces.

STEM analysis of the bulk and surface region of the two materials showed discernible differences. The bulk grain structure after the highest temperature anneal (1550° C/3 h) of the two materials is shown in Fig. 3. While the bulk grain-size distribution in the two materials is similar, the Hi-Sil grains were much more spherical. The surface grain structures of these materials were drastically different, Fig. 4. The Hi-Sil surface was composed of large 5 to 10 μm grains while the Lo-Sil surface retained its fine grain structure, except for an occasional large grain.

An XRF comparison of the polished as-fired surfaces of the two materials shows four times as much silica at the Hi-Sil material surface in comparison to the Lo-Sil. After annealing at 1550° C, the silicon content increased only slightly (within the error of our measurements) on the Lo-Sil surface while the silicon content of the Hi-Sil surface doubled. This increase in silicon at the surface coincided with surface yttria enrichment. The effect of silica content on the yttrium migration was further investigated by adding silica to the Lo-Sil material and annealing at 1550° C/3 h. Consequently, two batches of co-precipitated Y–TZP were made from ZrOCl with different silica contents and treated similarly. The high-purity ZrOCl had less than 1 p.p.m. of any impurity, including iron, aluminium, sodium and calcium. The results of an XRF analysis of the YL line are shown in Table II. The effect of increasing silica in both the Lo-Sil and co-precipitated material was to greatly increase yttrium migration. Samples of Hi-Sil and Lo-Sil were subsequently annealed for 20 h at 1450 and 1550° C to test whether the enrichment had a limiting composition or continued until the interior is depleted of silica and yttria. Table III shows the resulting data; no change in surface yttria or silica content was seen during the extended anneal. The yttrium transfer was essentially complete after 3 h at each temperature.

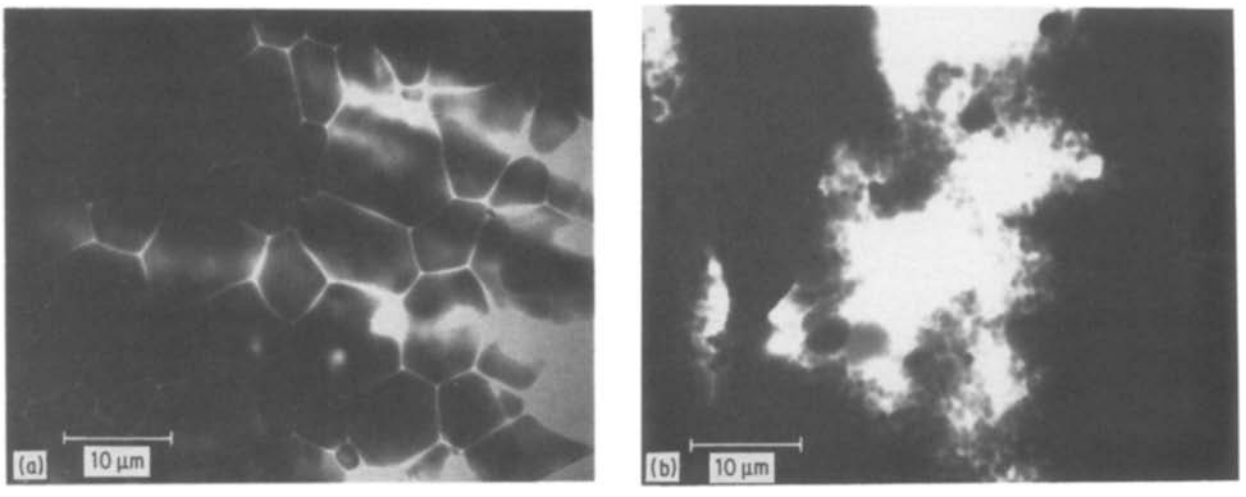

Figure 4 Microstructure of surface region of samples annealed at 1550° C for 3 h: (a) Hi-Sil, (b) Lo-Sil.

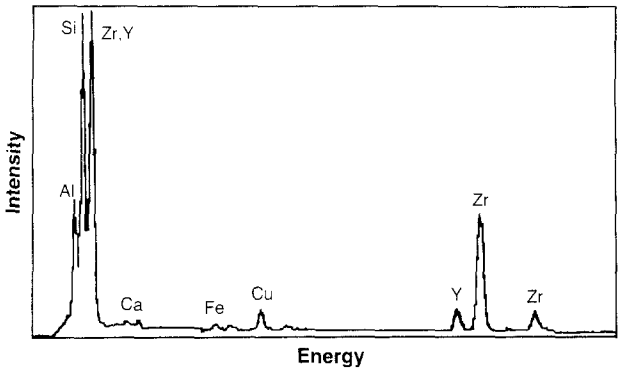

Figure 5 EDX spectrum of grain boundary in Hi-Sil Y–TZP.

The role of small grain-boundary concentrations of other impurities in silica migration has not been clearly established. Recently, Drennan and Hannink [2] have shown that small amounts of SrO cause the silicate glassy phase to be ejected to the surface in Mg–PSZ. Chaim *et al.* [3] have seen large concentrations of impurities, especially iron, in the grain boundaries of sintered Zircar material. Our EDX spectra of grain boundaries in the annealed Zircar (Hi-Sil) material showed little or no presence of active surface elements (iron, strontium, chromium, nickel) in any significant amount, Fig. 5. The yttrium content in the grain boundaries of the surface and bulk regions was also studied during TEM analysis of a Hi-Sil sample annealed at 1550° C/3 h. There was much less yttrium in the grain boundaries at the surface than in the bulk. This indicates that yttrium, which is dissolved in the glassy phase in the bulk, diffuses back into the grains at the surface.

The difference in surface yttria content and grain structure of the two materials was also reflected in the

TABLE II Effect of silica on yttria migration

Material	SiO_2^* (wt %)	Surface Y_2O_3 (wt %)	
		As-fired	Annealed 1550° C/3 h
Lo-Sil	0.008	4.5	5.0
Lo-Sil + SiO_2	0.048	4.5	8.1
Co-precipitated	0.070	4.3	7.5
C.P. high purity	0.010	5.1	5.2

*Silica contents based on Lo-Sil 0.008 wt % SiO_2 as a standard.

XRD patterns shown in Figs 6a and b. These patterns demonstrate that the Hi-Sil surface, which contained about 9.0 wt % Y_2O_3 (by XRF *L*-line analysis) after annealing, had developed a significant amount of a second phase. These samples were not quenched so this region contains both a tetragonal (t′) and cubic phase, in addition to the original tetragonal phase [4]. An XRD pattern of a bulk 8 wt % Y_2O_3 Zircar sample shows a similar phase composition, Fig. 7. Using Scott's [5] lattice parameter data and a mass balance, the yttria concentration of the t phase and t′ cubic phase were about 4 and 10.4 wt % Y_2O_3, respectively. TEM analysis of the Hi-Sil confirms the presence of large grains containing ~10 wt % Y_2O_3 and small grains containing 4 to 4.5 wt % Y_2O_3. The t and t′ segregation was also observed on the Lo-Sil surface but to a much lesser degree. These phases were still present after the annealed surface was removed by polishing.

These studies show that there are two effects occurring simultaneously during high-temperature annealing. One is the partitioning of the Y–TZP into yttria-rich and yttria-poor phases, which is expected from the phase diagram. The other effect is the non-

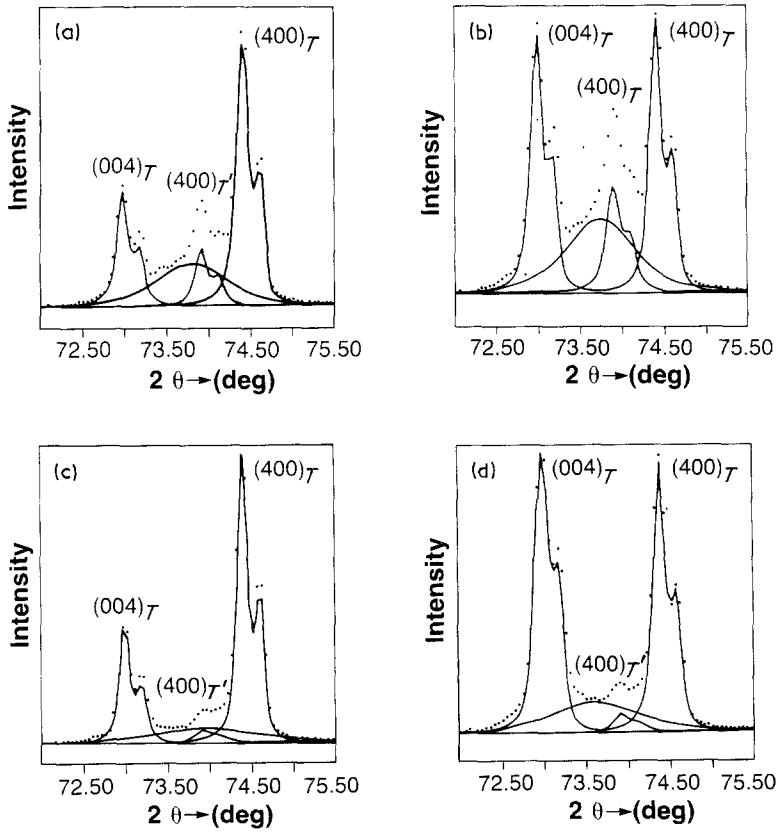

Figure 6 XRD patterns of Y–TZP surfaces annealed at 1550° C for 3 h: (a) Hi-Sil polished, (b) Hi-Sil ground. (c) Lo-Sil polished, (d) Lo-Sil ground.

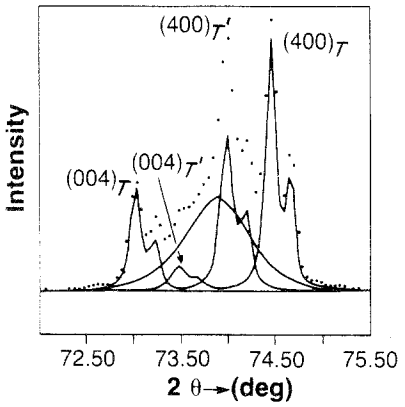

Figure 7 XRD patterns of an 8 wt % Y_2O_3/ZrO_2 bulk Zircar sample.

equilibrium migration of yttria to the surface which causes both microstructural and enhanced phase changes, and is greatly facilitated by the presence of silica in the grain boundaries. These surface effects have been recently reported by Lange *et al.* [6] and Chaim *et al.* [3] but the distinct roles of yttria migration and phase segregation were not clearly identified.

4. Conclusion

A surface-sensitive XRF technique was used to analyse the chemical changes occurring during the high-temperature anneal of Y–TZP. The yttria and silica content of the surface region increased with increasing annealing temperature. One of the controlling factors determining the extent of the yttria enrichment was the degree of silica present in the fired material. The surface treatment before annealing also had an effect on the extent of yttria enrichment. The results of XRD and TEM analysis support these conclusions by providing detailed results of phase compositions and microstructure.

TABLE III Effect of long-time, high-temperature anneal on yttria migration

Material	As-fired	Surface Y_2O_3 (wt %)			
		1450° C		1550° C	
		3 h	20 h	3 h	20 h
Lo-Sil	4.5	5.0	4.9	5.0	4.7
Hi-Sil	4.8	7.4	7.4	8.9	8.3

References

1. M. MATSUI, T. SOMA and I. ODA, in "Advances in Ceramics", Vol. 12, "Science and Technology of Zirconia II", edited by N. Claussen, M. Ruhle and A. Heuer (American Ceramic Society, Inc., Columbus, Ohio, 1984) pp. 371-81.
2. J. DRENNAN and R. H. J. HANNINK, *J. Amer. Ceram. Soc.* **69** (1986) 545.
3. R. CHAIM, D. G. BRANDON and A. H. HEUER, *Acta Metall.* **34** (1986) 1936.
4. V. LANTERI, A. H. HEUER and T. E. MITCHELL, in "Advances in Ceramics", Vol. 12, "Science and Technology of Zirconia II", edited by N. Claussen, M. Ruhle and A. Heuer (American Ceramic Society, Inc., Columbus, Ohio, 1984) pp. 118-30.
5. H. G. SCOTT, *J. Mater. Sci.* **10** (1975) 1529.
6. F. F. LANGE, H. SCHUBERT, N. CLAUSSEN and M. RUHLE, *ibid.* **21** (1986) 768.

Received 24 February
and accepted 29 April 1987